3D porous nanostructured platinum prepared using atomic layer deposition

3D Porous Nanostructured Platinum Prepared using Atomic Layer Deposition

S. P. Sree,[a†] J. Dendooven,[b†] L. Geerts,[a†] R. K. Ramachandran,[b] E. Javon,[c] F. Ceyssens,[d] E. Breynaert,[a] C. E. A. Kirschhock,[a] R. Puers,[d] T. Altantzis,[c] G. Van Tendeloo,[c] S. Bals,[c] C. Detavernier[b] and J. A. Martens*[a]

Received 00th January 20xx,
Accepted 00th January 20xx

DOI: 10.1039/x0xx00000x
www.rsc.org/

A robust and easy to handle 3D porous platinum structure was created via replicating the 3D channel system of an ordered mesoporous silica material using atomic layer deposition (ALD) over micrometer distances. After ALD of Pt in the silica material, the host template was digested using hydrogen fluoride (HF). A fully connected ordered Pt nanostructure was obtained with morphology and sizes corresponding to that of the pores of the host matrix, as revealed with high-resolution scanning transmission electron microscopy and electron tomography. The Pt nanostructure consisted of hexagonal Pt rods originating from the straight mesopores (11 nm) of the host structure and linking features resulting from Pt replication of the interconnecting mesopore segments (2-4 nm) present in the silica host structure. Electron tomography of partial replicas, made by incomplete infilling of Zeotile-4 material with Pt, provided insight in the connectivity and formation mechanism of the Pt nanostructure by ALD. The Pt replica was evaluated for its potential use as electrocatalyst for the hydrogen evolution reaction, one of the half-reactions of water electrolysis, and as microelectrode for biomedical sensing. The Pt replica showed high activity for the hydrogen evolution reaction and electrochemical characterization revealed a large impedance improvement in comparison with reference Pt electrodes.

Introduction

Platinum nanostructures exposing large surface area are required for miniaturized sensing and electronic devices.[1] The synthesis of platinum nanostructures is challenging as the high surface energy of platinum metal favors low rather than high specific surface area. Platinum nanoparticles with desired size and shape can be obtained via colloidal chemistry approaches using capping agents to achieve steric or electrostatic stabilization.[2,3] These nanoparticles can be fixed at surfaces or assembled to generate larger features. An early means to achieve porous platinum nanostructures is de-alloying, whereby the less noble metal is selectively leached from a bimetallic alloy via an electrochemical or chemical process.[1,4,5] Another strategy for achieving platinum nanostructures makes use of the soft templating approach where surfactant self-assembly generates ordered platinum structures constituting walls separating regular voids holding the soft template such as e.g. a lyotropic liquid crystal (LLC) phase of octaethylene glycol monohexadecyl ether [6,7] or diblock copolymer[8–10]. Various morphologies were prepared by electrochemical or chemical reduction of the platinum precursor and removal of the surfactant.[7,9] Synthesis of porous platinum with large mesocages using electrodeposition templated by poly(styrene-b-ethylene oxide) block copolymer has been demonstrated.[10] Platinum nanoballs, containing 50-80 nm mesodomains of connected nanowires, were generated by use of giant hexagonal mesophases with cetyl trimethyl ammonium bromide as soft template.[9]

Another efficient methodology to realize mesostructured Pt is hard templating, which is based on the deposition of the metal in the pores of a mesoporous oxide matrix followed by dissolution of the hard template to liberate the metallic replica.[1] Electrodeposition of platinum in the pores of anodic aluminum oxide (AAO) templates resulted in solid nanowires with diameters according to the AAO pore size.[11–14] Deposition on the walls of AAO pores resulted in the formation of hollow platinum nanotubes. An alternative attractive robust hard template is ordered mesoporous silica.[1,15–17] Replicas of many ordered mesoporous silica matrices have been reported, most appearing like networks of polycrystalline nanowires.[18–24] Olive shaped porous Pt metal bodies of 150 to 230 nm with an internal structure of interconnected Pt nanorods were created using SBA-15 template.[25] Formation of single-crystal platinum nanorods by glycol-assisted one step vacuum impregnation of SBA-15 template was reported. Depending on the Pt precursor concentration, either individual nanorods or interconnected nanorod bundles were obtained.[26] Gyroid Pt nanowire networks were obtained by replication of the pores of MCM-48.[27] The double gyroid structure of KIT-6 was replicated to form an inverse gyroid structure with average particle sizes of 50 nm to a few hundred nanometers.[17,28]

Impregnation of a Pt complex in the pores of a hard template followed by chemical or electrochemical reduction and template dissolution is the most common pore replication method.[1,17–24,28–33] Photoreduction is an alternative to (electro)chemical reduction.[15,16] Atomic Layer Deposition (ALD) is a technique which proved its efficiency in introducing metal and metal oxides into mesoporous silica matrices,[34–36] but ALD of platinum for the creation of porous nanostructures has scarcely been reported. For instance, nanostructured films composed of Pt/Ir nanowires (~ 70 nm diameter) via ALD into AAO membrane have been reported.[37] In

[a.] *Center for Surface Chemistry and Catalysis, KU Leuven, Celestijnenlaan 200F, Leuven B-3001, Belgium*
[b.] *Department of Solid State Sciences, UGent, Krijgslaan 281/S1, B-9000 Gent, Belgium*
[c.] *EMAT, University of Antwerp, Groenenborgerlaan 171, B-2020 Antwerp, Belgium*
[d.] *Department of Electrical Engineering (ESAT), Kasteelpark Arenberg 10, B-3001, Belgium*
† Authors with equal contribution

Electronic Supplementary Information (ESI) available: [A movie showing the 3D porous structure of the Zeotile-4 and the corresponding replica which demonstrating the replication of the pore system of host matrix by platinum] DOI: 10.1039/x0xx00000x

that study, after ALD of Pt and Ir, the AAO membrane was epoxy-bonded to a polycarbonate substrate whereafter the hard AAO template was etched in alkaline solution to liberate the Pt/Ir film. Also a low temperature ozone-based Pt-ALD process was demonstrated, by which anodized alumina pores with an average diameter of 23 nm and mesoporous silica films with a much smaller average pore diameter of 4 nm could be coated conformally.[38] Applying the same process on ordered multi-walled carbon nanotubes followed by removal of CNTs created a 3D network of self-supporting Pt nanowires.[39] Further, ALD was used to investigate the growth of Pt nanostructures on highly ordered pyrolytic graphite model carbon surface forming laterally aligned Pt nanowires.[40]

Nanostructured platinum materials fire the imagination of designs for tailor-made metal catalysts, electronics, non-linear optics and magnetic devices.[41] Efforts are reported in literature where the purpose of making a Pt replica was mainly to reveal the pore architecture of the hard template material, as Pt nanostructures are conveniently imaged via electron microscopy.[18–20] The existence of connecting micropores between mesopores of SBA-15 material was revealed using a Pt replica.[24] Platinum nanowires and nanoparticles templated on FSM-16 and HMM-1 have been tested for the preferential oxidation of CO in H_2 excess, which is important in fuel cells, where trace amounts of residual CO can poison the electrodes. A high activity and selectivity has been reported for the nanowires and particles in FSM-16.[16] Moreover, a high catalytic performance for the water gas shift reaction has been demonstrated on Pt wires templated inside FSM-16 pores.[42] Pt nanowires made in AAO membranes have been reported to function well in hydrogen peroxide detection.[11] Nanowire arrays, fabricated using the electrochemical deposition of PtCu alloy nanowires onto AAO templates followed by de-alloying of the Cu component, have been investigated for ethanol electro-oxidation, a half-reaction of ethanol fuel cell.[43] Skeletal Pt nanostructures, prepared through the chemical reduction by ethylene glycol vapor of a Pt precursor in presence of $(NH_4)_2CO_3$, exhibit high activity for the electrochemical oxidation of methanol.[44]

Reported Pt nanostructures are mostly nanowire assemblies, made using channel type host matrices. Also with the current methods it appears very difficult to replicate the hard porous template over lengths exceeding a micrometer. Such larger structures are desired for electrode and sensor applications. Here we report the fabrication of large skeletal platinum structures by replication of an ordered mesoporous 3D mosaic structure called Zeotile-4. It is formed by tiling of pre-fabricated rectangular silica particles, designated as nanoslabs (4*8*2 nm^3), in a hexagonal pattern.[45–47] The unique skeletal 3D porous mosaic Pt structure was confirmed with electron tomography. Electrochemical characterization revealed exceptional properties.

Experimental

Synthesis of Zeotile-4

Zeotile-4 powder was synthesized following a recipe reported in ref [47]. This involved the preparation of a clear solution of silicalite precursors otherwise called silica nanoslabs and combining it with Pluronic 123 followed by aging at high temperature. The clear solution was prepared by mixing tetra-ethylorthosilicate (TEOS) with tetrapropylammonium hydroxide (TPAOH) under vigorous stirring facilitating the hydrolysis of TEOS. Then water was added to the suspension and stirred for another 24 hrs. The molar ratio of TEOS: TPAOH: H_2O was maintained to be 25: 9: 400. 18 g of this clear solution was added to 9 g HCl (5M) and mixed with 24 g of aqueous Pluronic P123 solution (10 wt %) which has been already acidified using 8 g of 5 M HCl. The mixture was kept at 95 °C for 96 h in a polypropylene bottle. The solid precipitate formed was recovered, washed, dried and calcined at 350°C for 12 h using a heating ramp of 0.5°C/min.

Atomic Layer Deposition

Pt-ALD was carried out in a home built cold wall ALD chamber.[38] The powder sample was loaded in a molybdenum sample cup, which was then transferred into the ALD reactor through the load-lock and was placed on a heater block. The sample was then allowed to outgas and thermally equilibrate for at least 1 h under vacuum. The solid $MeCpPtMe_3$ precursor (99% Strem Chemicals), kept in a stainless steel container, was heated above its melting point (30 °C), and the delivery line to the chamber was heated to 60 °C. Argon was used as a carrier gas for the Pt precursor. O_3 was produced from a pure O_2 flow with an OzoneLabTM OL100 ozone generator, resulting in an O_3 concentration of 175 µg/ml. A static exposure mode was applied during both ALD half-cycles. The pulse time of the MeCpPtMe3 precursor was 10 s, after which the valves to the pumping system were kept closed for another 20 s, resulting in a total exposure time of 30 s. The same pulse time and exposure time was used for the O_3 also. For the creation of the full replica (Figure 3), the $MeCpPtMe_3$ precursor exposure was repeated 3 times for one O_3 exposure during each ALD cycle. For the creation of the micron-long mesoporous Pt tubes (Figure 6), only one precursor pulse was applied during each ALD cycle. In both cases, 250 ALD cycles were applied. During the precursor and reactant exposures, the pressure in the chamber increased to *ca*. 0.5 mbar and 1 mbar, respectively. After ALD, the silica of the host material was digested using 0.5 M HF solution at 60 °C for 3 h to create the Pt replica.

HR-SEM

HR-SEM images of all samples were obtained on a Nova NanoSEM450 (FEI, Eindhoven). The powder samples were mounted on aluminium stubs using carbon tape and directly imaged without any further sample modification.

TEM / Tomography

HAADF-STEM images, electron tomography series and selected area electron diffraction (SAED) patterns were acquired by using an aberration corrected 'cubed' FEI Titan electron microscope operated at 200 and 300 kV. Electron tomography series acquisition was performed in STEM mode by using a Fischione model 2020 single tilt tomography holder. The series was reconstructed by using the simultaneous iterative reconstruction technique (SIRT) implemented in the Inspect3D software from FEI.

N_2 physisorption

N_2 physisorption measurements were performed on a Quantachrome Autosorb-1. The samples were pretreated at 120 °C under vacuum for 12 h. The N_2 adsorption isotherms were analyzed using Brunauer–Emmett–Teller (BET) and t-plot methods.

Synthesis of Hydrogen Evolution Electrode

N-type silicon wafers (Cemat Silicon, 4" unpolished) with a thickness of 525-575 µm were used as substrates for the Pt deposited Zeotile-4. RCA cleaning was performed and followed by a wet oxidation at 1100 °C for 2 h which resulted in an insulating layer of SiO_2. Thin film layers were sputtered with a Balzers BAE 370 sputtering tool. A Ti/W ($Ti_{10}W_{90}$ target, 99.95%) was sputtered at 2.10^{-3} mbar and 150 W for 1 min as an adhesion layer for the platinum metal. Pt (Pt target, 99.95%) was then sputtered at 100 W for 3 min under Ar atmosphere at 2.10^{-3} mbar. Subsequently a conducting wire was soldered on the electrode by use of silver paint (RS, US) and the contact was sealed with epoxy coating (Hysol 9466, Henkel). Geometric surface areas were determined by making a picture of the electrodes and using the software ImageJ to calculate the area. Prior to deposition, the substrate was cleaned in milliQ water and ethanol. To make a catalyst ink, the powder with Pt (0.0114 g) was dispersed in 2 ml ethanol with 0.0209 g polyvinyl alcohol (Sigma-Aldrich) and 30 µl nafion (Sigma-Aldrich). The solution was intensively vortexed to become a homogenous solution. The replica was deposited on precleaned platinum support by use of a micropipette. 6 times 5 µl was pipetted on the surface. The electrodes were then air-dried for 60 ± 10 min.

Electrocatalytic activity for the Hydrogen Evolution Reaction

Current-voltage curves were recorded without IR compensation at ambient temperature using a VersaSTAT 4 potentiostat (Princeton Applied Research) in a one-compartment electrochemical cell with electrolyte content of approximately 600 ml. Experiments were performed in 0.5 M H_2SO_4 and the electrolyte (Fisher Scientific, 95%) was diluted at 0.5 M concentration using Milli-Q water (18 MΩ cm). A platinum ring served as auxiliary electrode and an Ag/AgCl (3M KCl saturated with AgCl, Radiometer Analytical) was used as reference electrode. Scan rate was set at 2 mV/s and H_2 was purged through the solution prior to measurements to saturate the solution.

Fabrication of multi-electrode array

A multi-electrode array of flat circular test electrodes with 0.019 cm^2 surface area was fabricated by lithography on a glass substrate. A two-layer lift-off resist layer (LOR10B + S1818) was applied by spin coating and patterned by UV contact lithography and development in 0.26N NaOH. 10 nm thick TiW adhesion layer and a 120 nm thick Pt layer were sputtered with a Balzers BAE 370 sputtering tool, after which the remaining lift-off resist was removed in N-methylpyrrolidone. Next, a 5 µm thick film polyimide (Dupont PI-2611) was applied by spin coating and cured at 350 °C to serve as insulation layer. A reactive ion etch using a thick ma-p 1275HV resist layer as mask, was used to open the polyimide layer, thereby releasing the platinum layer and defining the size and shape of the electrodes.

The tubular Pt Zeotile-4 replica was dispersed in demineralized water at a concentration of 3 wt% and mixed by sonication. The resulting suspension was deposited on the test electrodes (heated to 90 °C to accelerate drying) by micropipetting 1 µL drops five times per electrode. The resulting layer was then annealed for 5 hours at a temperature between 250 and 575 °C (in Ar from 450°C on, to protect the polyimide from oxidation).

Impedance and charge injection capacity of multi-electrode array

Testing was performed in phosphate buffered saline water (Invitrogen Gibco, pH 7.2) using a platinum counter electrode and an Ag/AgCl electrode (3M KCl saturated with AgCl, Radiometer Analytical) as reference. The readout electronics consisted of a Solartron SI 1255 frequency response analyser and a SI 1287 electrochemical interface. For impedance testing, a 0.1 V amplitude sine waveform was scanned between 0.1 and 1MHz. For cyclic voltammetry, a scan rate of 100 mV/s was employed.

Results and discussion

Zeotile-4 is an ordered mesoporous material with parallel straight channels in hexagonal arrangement, interconnected systematically via slit-like voids left open between the stapled nanoslabs. The architecture of this nano-mosaic has been demonstrated earlier by electron tomography.[47] Zeotile-4 synthesis starts with the preparation of a suspension of nanoslabs from tetraethylorthosilicate (TEOS) and tetrapropyl ammonium (TPA) hydroxide.[45] Mesostructuring of the nanoslabs subsequently is achieved using triblock copolymer, Pluronic P123 surfactant. The organics are conveniently removed by calcination to evacuate the pores.

Zeotile-4 particles were investigated by scanning electron microscopy (SEM). Hereby, a concentric backscattered detector, combined with beam deceleration at accelerating voltages down to 500 V was used. The particles were found to adopt an hexagonal cylindrical morphology, with typical sizes of 2-3 µm by 0.5-1 µm (Figure 1). The systematic presence of two types of pore openings is revealed: *i*, openings of ~11 nm in an hexagonal arrangement

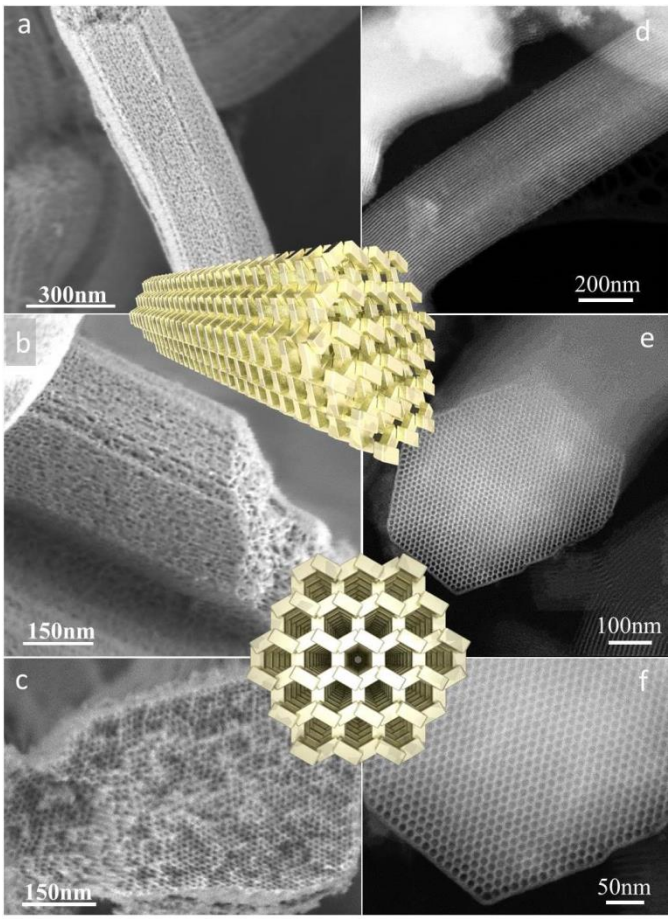

Figure 1 HR-SEM images of calcined Zeotile-4 sample: (a,b) lateral view showing the presence of slit like entrances allowing sideways access to the porosity and (c) axial view which presents hexagonally ordered mesopores of ~11 nm. HAADF-STEM images of calcined Zeotile-4 particles:. (d) lateral view and (e-f) view perpendicular to the main mesopores (~11nm) at different magnifications. Overlaid is the schematic of Zeotile-4 structure, (top) the lateral view and (bottom) the axial view.

observed at the end and ascribed to the apertures of straight mesopores running according to the long direction of the particles and *ii*, sideways perforation ascribed to the termination of the slit pores. A movie in the supplementary information shows the idealized topology of Zeotile-4 and the resulting replica (supplementary movie 1).

Zeotile-4 hard template with its 3D mesoporosity is particularly suited for ALD, as demonstrated previously for TiO_2 deposition.[36,47] In this work, Pt-ALD was performed on Zeolite-4 powder using alternating exposure to (methylcyclopentadienyl)trimethylplatinum ($MeCpPtMe_3$) vapor and O_3 gas at 200 ˚C.[38] Large precursor exposures were used to enhance the deposition in the inner portions of the Zeotile-4 material (see Methods Section). After 250 ALD cycles, the silica of the Zeotile-4 host material was dissolved using 0.5 M HF solution at 60 °C for 3 h to liberate the Pt replica. HAADF-STEM imaging confirmed the uniform dispersion of Pt on the Zeotile-4 powder particles (Figure 2a). Figure 2b shows an HR-SEM image of the Pt replica after dissolution of the hard template material. Comparison of Figure 2a, where the silica matrix is still present, with Figure 2b confirmed that the as-deposited structure is retained after removal of the template. Figure 2c and d show the

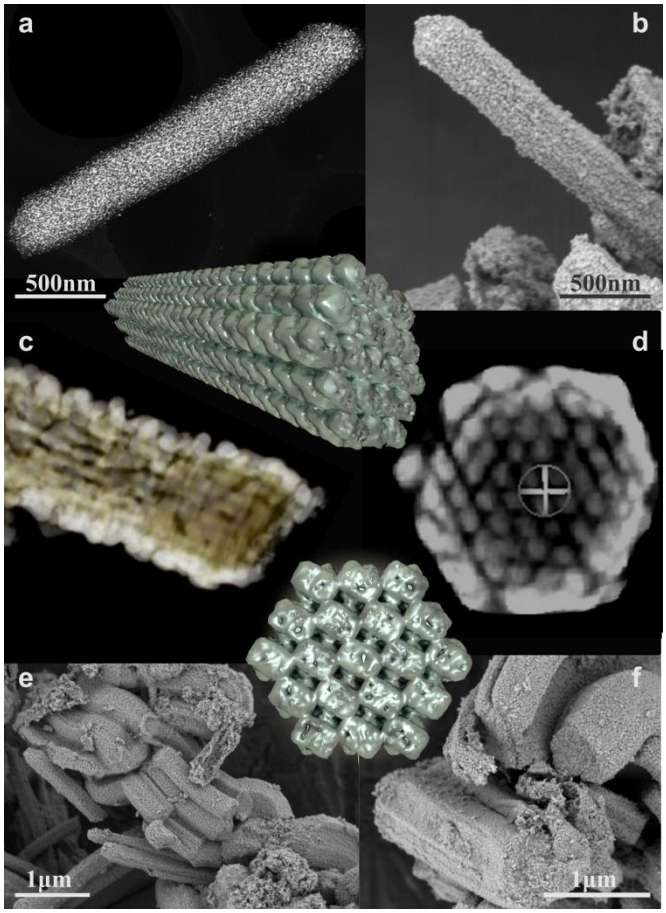

Figure 2 (a) HAADF -STEM image of Zeotile-4 filled with Pt and (b,e,f) HR-SEM images of Pt Zeotile-4 replica at different magnifications. (c,d) orthoslices of tomography sequences of the Pt replica (supplementary movies 2 and 3) Overlaid is the schematic of Pt replica structure, (top) the lateral view and (bottom) the axial view.

orthoslices of the tomography sequences (supplementary movie 2 and 3). The successful replication of the porous structure over micron lengths is demonstrated by the HR-SEM images in Figures 2 e and f. BET-analysis of the N_2 physisorption isotherms yielded a specific surface area of 20 m^2g^{-1}, confirming the formation of an open, accessible interior void structure. Values of 53 m^2g^{-1} and 38 m^2g^{-1} have been obtained respectively with unsupported Pt-nanowire networks based on a soft template,[29] and with inverse gyroid structures templated from KIT-6.[17] The Pt replica of Zeotile-4 was quite robust and survived mechanical processes like sonication, indicating firm connectivity of the rods and struts of the Pt nanostructure. No visible changes of the Pt morphology were observable in SEM after annealing of the Pt structure.

HAADF-STEM images of the Pt Zeotile-4 replica (Figure 3) allowed a more detailed characterization of the morphology of the obtained Pt nanostructure. The plan view images in Figures 3a and b revealed the formation of Pt rods along the long direction of the Zeotile-4 template as a consequence of the successful ALD filling of the straight Zeotile-4 mesopores with Pt. Moreover, these images evidenced the arrangement of Pt struts connecting the main rods. The cross sectional view of the Pt replica in Figure 3c provided confirmation of the hexagonal shape of the Pt rods and of the

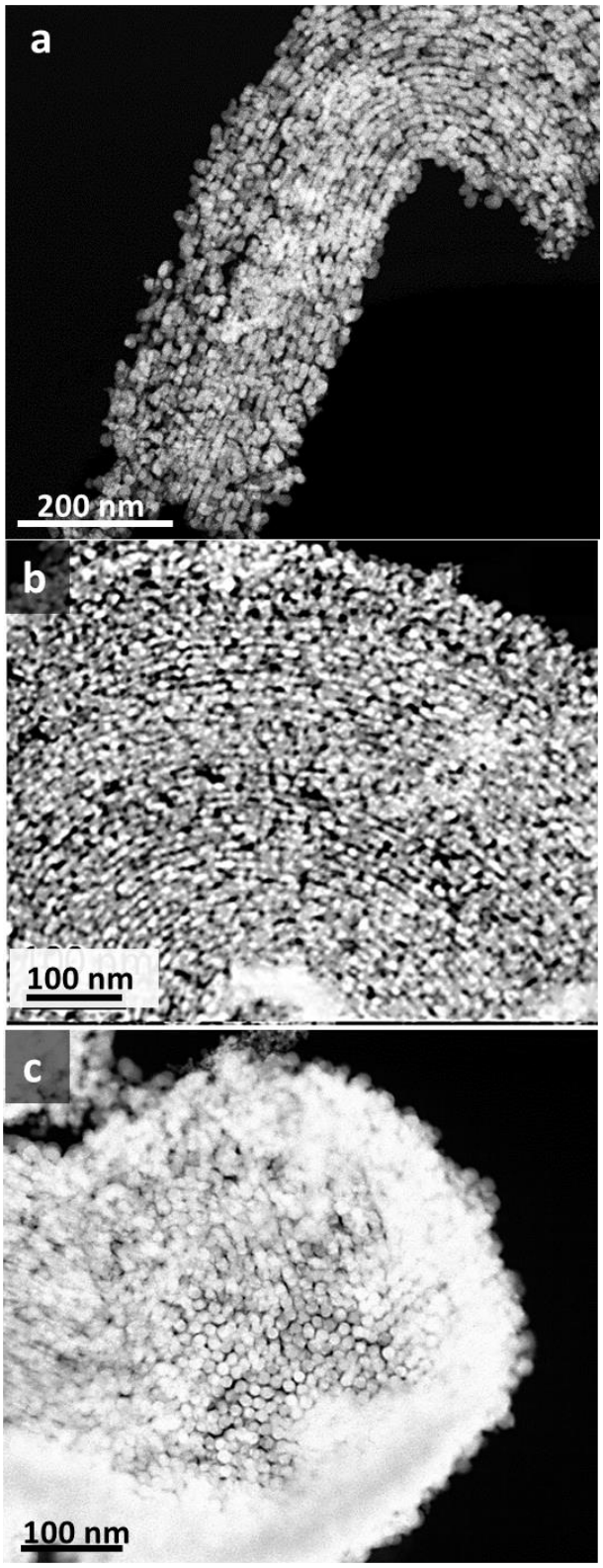

Figure 3 HAADF-STEM image corresponding to (a,b) plan view of the replica showing the struts of Pt and (c) cross-section of Pt replica after removing the silica with HF indicating the conservation of organization

overall hexagonal organization originating from the pore arrangement in the Zeotile-4 template. The diameter of the Pt rods

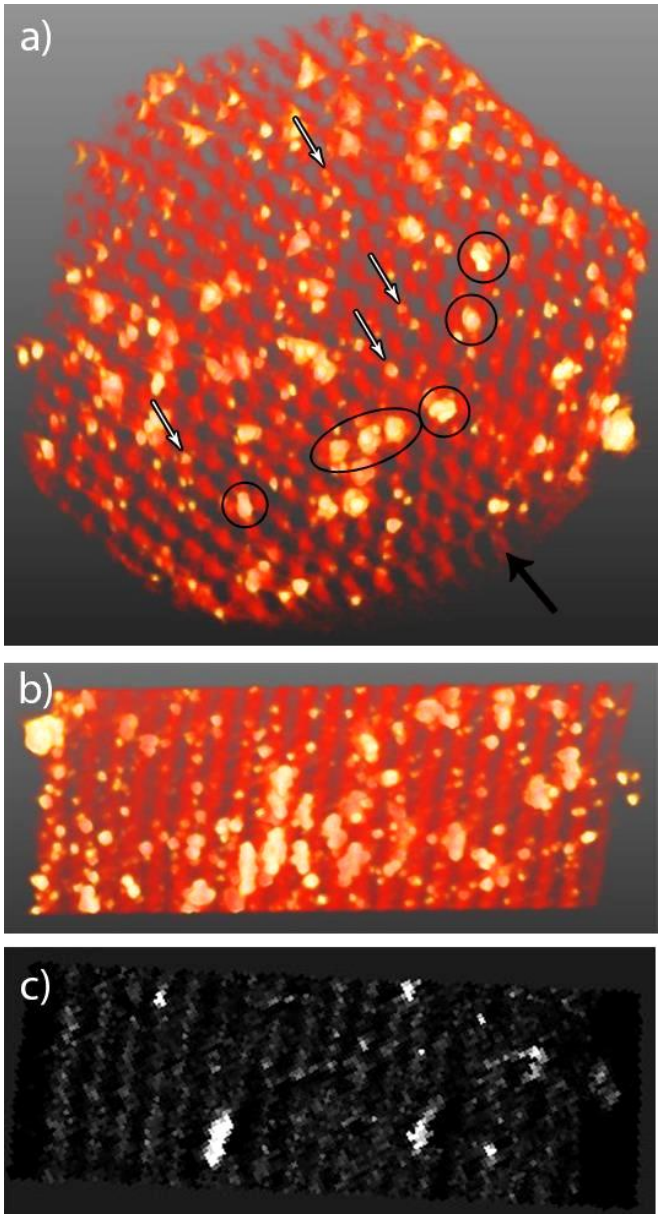

Figure 4 (a, b): volume rendering of the tomography reconstruction displayed along two directions. White arrows show the small aggregates of Pt localized between the slabs and black circles highlight large aggregates of Pt localized in the in the main mesopores . The black arrow indicates the direction along which the second orientation (b) is visualised. (c) Orthoslice showing localization of the large aggregates of Pt in the mesopores of the Zeotile-4

of the replica and the pores of the silica host material were identical, viz. 11 nm (Figure 1f).

To explore the matching of the embedded platinum nanostructure and the Zeotile-4 template, both phases need to be mapped during a same tomography series. Unfortunately, due to the large difference in atomic number for Pt and Si it was not possible to map the silica of Zeotile-4 by HAADF-STEM when the material is filled with Pt. Therefore, powder particles with reduced Pt loading via ALD were characterized with HAADF-STEM tomography. This study (Figure 4) revealed the formation of Pt aggregates, owing to the

nucleation-controlled growth mode of the Pt-ALD process.[38] Figure 4a and b present two different orientations of the volume rendering of the 3D reconstruction, and Figure 4c shows a slice though the reconstruction. In Figure 4a, the hexagonal organization of Zeotile-4 (red color) is recognized. Aggregates of Pt which are highlighted by a bright and yellow color are localized at different places. In this orientation the main channels of Zeotile-4 are interspaced with stacks of nanoslabs with slits in between them. Many of the smallest aggregates such as those shown by the white arrows, are observed inside the stacking of nanoslabs, indicative of Pt nucleation on the accessible nanoslab surfaces inside the small slits. Other small aggregates are localized in the large hexagonal pores created by the nanoslab organization, indicating that platinum particle growth can also start at the sides of the nanoslabs. Large aggregates such as those highlighted with black circles in the Figure 4a, are systematically located in the main channels. From the view in perpendicular direction (Figure 4b) it is also clear that these aggregates are elongated in the direction of the pores. A movie is available in the supplementary information, observing one large aggregate seen under different orientations (supplementary movie 4). The orthoslice shown in Figure 4c corresponds to a real section in the center of the sample. The lower contrast corresponds to the silica of Zeotile-4 and the highest contrast to the aggregates of Pt. Since it does not correspond to a projection, the orthoslice confirms the location of the large aggregates of Pt in the large channels of zeotile-4. Based on these results, we propose the following nucleation and growth mechanism for the Pt-ALD process in Zeotile-4 material. The presence of small Pt aggregates within the stacking of the slabs and along the walls of the main channels suggests that the nucleation of Pt particles can start anywhere on a nanoslab surface, and even more likely on the largest surface, which means inside the nanoslab stacking. Nucleation in the slit-like openings seems not be hindered by the limited size (2 to 4 nm) compared to the large straight channels (~11 nm). However, continued Pt deposition gives rise to bigger agglomerates that need larger space and only fit in the main channels of Zeotile-4. When the silica is removed by HF treatment in order to obtain the replica, rods of Pt grown in the main channels are held together by platinum struts formed by virtue of the nucleation of Pt nanoparticles in the nanoslab stacks. The robustness of the Pt replica is explained by this growth mechanism where there are no boundaries between Pt grown in the two types of pores. This growth model is further supported by High Resolution STEM on a completely filled sample (Figure 6b and c). It can clearly be seen that the platinum replica is composed of partially coalesced nanocrystallites, which presumably nucleated initially on the silica surface and grew during subsequent ALD cycles. Owing to the mild conditions of ALD with temperatures not higher than 200 °C the nanocrystallites did not fully merge into one solid structure but preserved their almost spherical habit. According to the corresponding electron diffraction these nanocrystallites are randomly oriented and do not show any significant alignment with respect to the original pore direction of the Zeotile, which also indicates the original orientation of each crystallite is preserved after nucleation, growth and coalescence with neighboring Pt particles. Interestingly the nanoparticles are stable in the porous silica matrix for at least 2-3 years and after silica removal, observed to be stable for months of storage at ambient conditions.

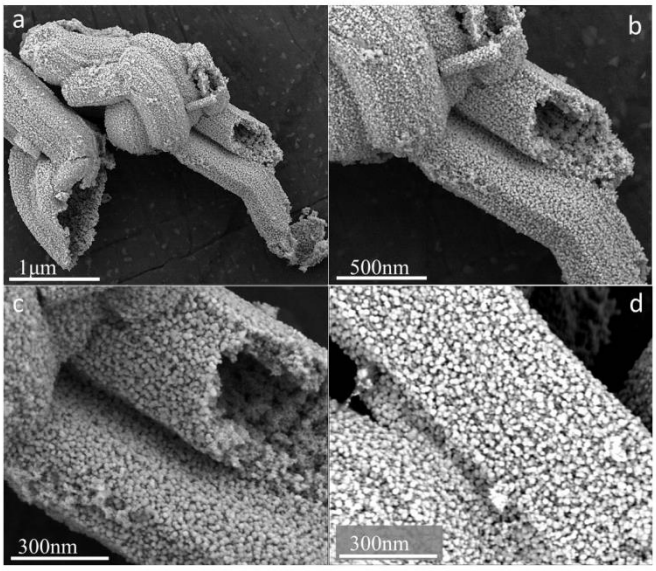

Figure 5 HR-SEM of Pt Zeotile-4 replica created via less time of exposure of the Pt precursor.

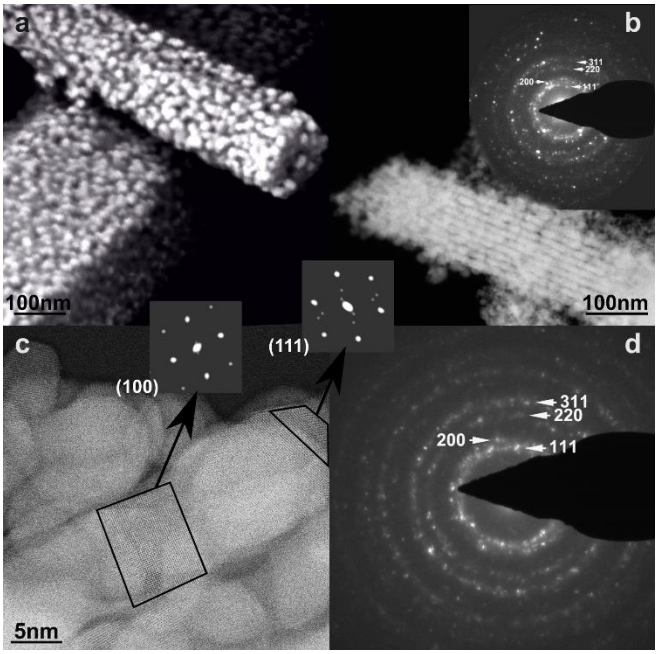

Figure 6 (a) HR-SEM of Pt Zeotile-4 replica. (b, c) HR-STEM of similar regions as shown in (a). (d) and inset in (b) show the electron diffraction patterns of (c) and (b) respectively. Small insets show contrast enhanced Fourier transforms with tentative assignment of the respective crystal facets of the regions indicated in c.

In previous work on TiO_2-ALD in Zeotile-4 powder particles, the TiO_2 deposition was concentrated in the rim of the Zeotile-4 particles by decreasing the exposure time of the Ti-precursor.[36] This could be understood based on the diffusion limited nature of the ALD process which leads to the progressive penetration of deposition fronts in all directions of the Zeotile-4 material with increasing exposure time. This property was exploited to create micron-sized mesoporous Pt tubes, which could be of interest for application. The penetration depth of the Pt precursor was limited by applying an ALD protocol with a three times shorter exposure time for the Pt precursor. The obtained Pt nanostructures liberated after silica dissolution in SEM had a nanoscopic appearance similar to the full replica (Figure 5). The large void in the middle of the replica confirmed the limited penetration depth of the ALD process in this instance. SEM (Figure 5b and c) evidenced the creation of Pt tubes of *ca.* 2 µm by 0.5 µm with a wall of thickness 150 nm and an inner diameter of ~200 nm. The wall thickness of the tube reflects the platinum deposition depth in the Zeotile-4 particles.[36] The presence of an open channel in the center of mesoporous Pt structure could be very beneficial to enhance the accessibility of the inner surfaces of the Pt structure. Using the diffusion-limited nature of ALD, the diameter of the open channel can be precisely tuned by changing the Pt precursor exposure time.

To illustrate the applicability of the Pt replica structure, proof-of-concept experiments were performed, being the application in electrocatalysis for the hydrogen evolution reaction (HER) and in biomedical sensing as microelectrode. Electrocatalysis is expected to take advantage of the large surface area exposed by the Pt replica. The activity of Pt replica electrode was investigated for the HER, one of the half-reactions of water electrolysis. To date, platinum is acknowledged as the most active HER catalyst with lowest overpotential.[48–50] Nanostructuring is a way to reduce the platinum content of electrodes.[48–51] A Pt replica electrode was prepared by depositing Pt replica powder on a 2.1 cm^2 flat platinum support via dropcasting (80 µg/cm^2). All electrochemical measurements were performed in 0.5 M H_2SO_4 at room temperature (21°C) using a one-compartment three-electrode electrochemical cell. Figure 7 shows the HER activity of the bare platinum support in comparison with the replica coated electrode.

The nanostructured Pt occluded in the Zeotile matrix has a significant catalytic activity towards the HER. Compared with the flat Pt support, the Pt replica coated electrode exhibits a higher current density and this was achieved with a loading of Pt on Zeotile-4 of ca. 80 µg/cm^2, representing ca. 55 µg/cm^2 platina. Typical loadings for the cathode side vary between 0.5 and 1 mg/cm^2.[52] The platinum replica coated electrode requires an overpotential of 120 mV necessary to drive the current density to 10 mA/cm^2, which is 45 mV less than for the flat Pt support. This significant enhancement indicates a very high mass activity of the Pt

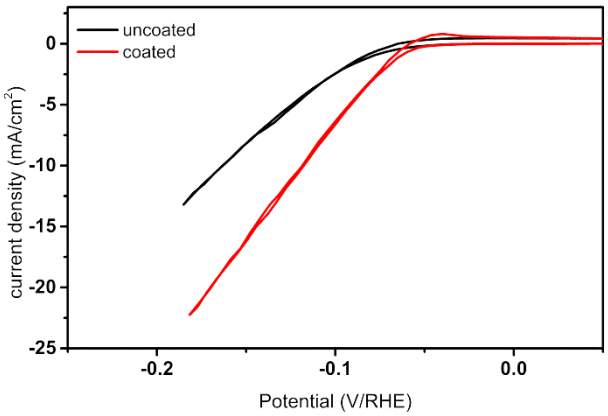

Figure 7 Cyclic voltammograms of the bare platinum support and Pt Zeotile-4 coated electrode. The potential (V/RHE) is the potential of the working electrode with respect to the reversible hydrogen electrode. The current density (mA/cm^2) is normalized to the geometric surface area. Scan rate was set at 2 mV/s.

nanostructure. Furthermore the electrode showed a stability. Seven cyclic voltammograms were recorded and the hydrogen evolution current density shows negligible change.

Single-crystal model experiments and computational studies revealed (electro)catalytic activity to be strongly dependent of atomic organization at the surface.[53–57] Close-packed low-index crystal planes such as (111) and (100) planes exhibit lower reactivity in comparison with (110) planes and planes with higher indices.[55–58] Increased reactivity was observed by the presence of steps, kinks and defects on these more open crystal surfaces. The mild temperature (200°) of the Pt-ALD process as well as the structure being composed of partially coalesced nanoparticles might explain why less stable crystal facets, like (100) are preserved (Figure 6). For very small Pt-nanoparticles it is known that energetically less stable faces than (111) can be expressed to minimize exposed surface by assuming an almost spherical rounded shape.[59]

In literature, colloidal synthesis has been applied for platinum particle synthesis with high index facets.[60,61] Nanosized cubes, tetrahedra and octahedra have been obtained.[57,62] Using multi-walled carbon nanotube support, Pt nanoparticles with higher fractions of high-index facets have been synthesized.[63] Electrochemical methods have been used for synthesis of particles with high-index facets by starting from conventional Pt nanocrystals and subjecting them to square-wave voltammetry.[64] After colloidal synthesis methods, ligands must generally be eliminated prior to use as electrocatalyst and this often results in altered size and shape. In this respect, impregnation of a template with a precursor, followed by gas- or liquid phase reduction is easier, but size and dispersion are more difficult to control.[63]

The hierarchical nature of the Pt nanostructure is expected to be beneficial to electrode impedance at relevant frequencies and charge injection capacity, two parameters that are important in the design of neural stimulation and recording implants. Pt replica powder was used to fabricate a platinum microelectrode. A planar platinum multi-electrode array of which each electrode has an area of 1.9 mm^2, was fabricated using standard lithography and thin film deposition techniques. Glass was used as substrate. Above, Pt was sputterdeposited and the microelectrodes were structured in a lift-off process. The process is detailed in the Methods section. An amount of 15 µg of Pt replica powder was deposited from suspension by micropipetting on each 1.9 mm^2 electrode, followed by heat treatment. Inspection by SEM confirmed the replica structure was preserved. Impedance spectroscopy and cyclic voltammetry in phosphate buffered electrolyte (pH 7.2) were used to assess performance and to compare to other Pt electrodes. Impedance spectroscopy (Figure 8a) shows that deposition of Pt replica reduces impedance in the low frequency (capacitively-dominated) part of the spectrum with three orders of magnitude. It had at least 5 times lower impedance than porous platinum electrodes based on platinum black from literature that were prepared via electroplating. This confirms the vastly enlarged accessible surface area. This confirms the vastly enlarged accessible surface area. [65–67]

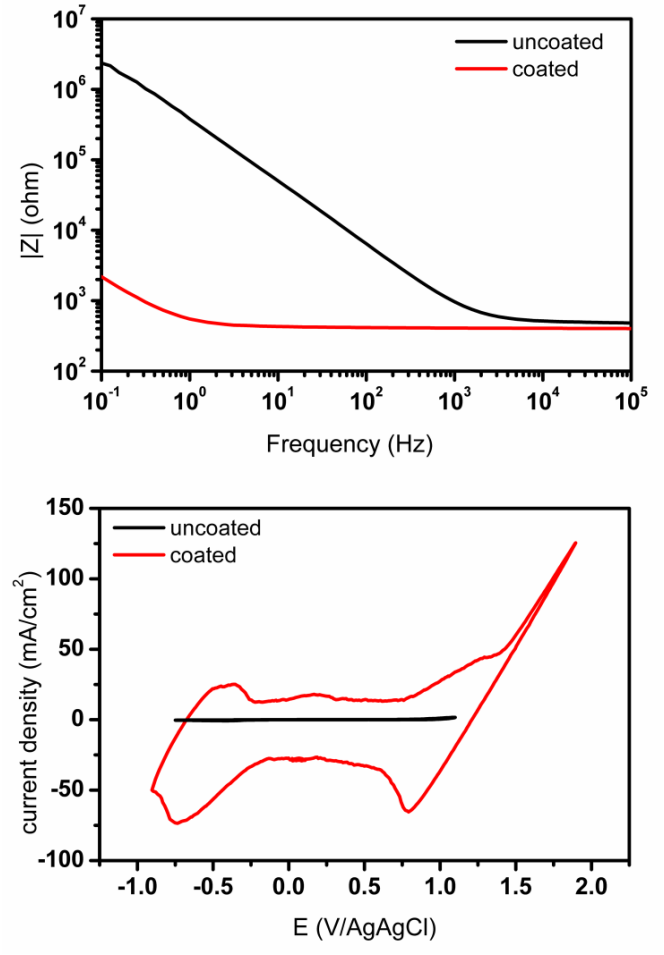

Figure 8 (a) Impedance spectra of Pt electrode (0.019 cm^2 surface area) with and without Pt replica deposited. Deposition of the Pt replica reduces the impedance in the low frequency region. (b) Cyclic voltammetry was performed at 100 mV/s. The potential is calibrated against the Ag/AgCl reference electrode and current density is normalized to geometric surface area. Charge storage capacity was increased by a factor of 230.

Cyclic voltammetry is used for determining the charge injection capacity, which is the time integral of the current at a certain sweep rate. Such a measurement on the 1.9 mm^2 Pt replica coated electrode showed 230 times increased charge storage capacity compared to flat Pt support (Figure 8b). This leads to the conclusion that Pt replica of Zeotile is a promising material for the fabrication of sensitive platinum electrodes, with potential biomedical applications such as neuro stimulation. Existing technologies include the use of porous platinum,[65,66] porous iridium oxide (deposited as such or electrochemically created in a smooth layer by anodization),[68] TiN,[66,69] carbon-based electrodes such as CNTs[70] or conductive polymer based electrodes such as PEDOT[71]. platinum replica of Zeotil-4 realized via ALD adds a new promising method.

Conclusions

Synthesis of interconnected hexagonal Pt nanorods by replicating the voids of a mesoporous Zeotile-4 template using atomic layer deposition was achieved. The Pt nanostructure measuring typically 2-3 µm by 0.5-1 µm consists of hexagonal Pt rods, matching with the straight pores of Zeotile-4 and linking features ascribed to Pt replication of interconnecting slits. The unique skeletal 3D porous mosaic Pt structure was confirmed with electron tomography. We developed a method that can replicate the hard porous template over lengths exceeding a micrometer, which is convenient for electrode and sensor applications. This structure has been shown to have a high activity for the hydrogen evolution reaction and to be promising for low impedance coatings for neural recording and stimulation electrodes, due to its large impedance improvement and high charge injection capacity. These enhanced properties could be attributed to the three-dimensional, ordered, mesoporous structure with large surface area, which can offer advantages in a wide range of applications. Future efforts can be devoted to the replication of other Zeotiles and mesoporous silica thin films. [46,72]

Acknowledgements

This work was supported by the Flemish government through long-term structural funding (Methusalem) to JAM and FWO for a research project (G0A5417N). JD, TA and FC acknowledge Flemish FWO for a post-doctoral fellowship. S.B. acknowledges funding from ERC Starting Grant COLOURATOMS (335078).

Notes and references

1 Y. Xu and B. Zhang, *Chem. Soc. Rev.*, 2014, **43**, 2439–2450.
2 B. Escobar Morales, S. A. Gamboa, U. Pal, R. Guardian, D. Acosta, C. Magana and X. Mathew, *Int. J. Hydrogen Energy*, 2010, **35**, 4215–4221.
3 Z. Peng and H. Yang, *Nano Today*, 2009, **4**, 143–164.

4 M. Oezaslan, M. Heggen and P. Strasser, *J. Am. Chem. Soc.*, 2012, **134**, 514–524.
5 S. Tominaka, M. Shigeto, H. Nishizeko and T. Osaka, *Chem. Commun.*, 2010, **46**, 8989–8991.
6 G. S. Attard, J. M. Corker, C. G. Göltner, S. Henke and R. H. Templer, *Angew. Chem. Int. Ed. Engl.*, 1997, **36**, 1315–1317.
7 G. S. Attard, P. N. Bartlett, N. R. B. Coleman, J. M. Elliott, J. R. Owen and J. H. Wang, *Science*, 1997, **278**, 838–840.
8 S. C. Warren, L. C. Messina, L. S. Slaughter, M. Kamperman, Q. Zhou, S. M. Gruner, F. J. DiSalvo and U. Wiesner, *Science*, 2008, **320**, 1748–1752.
9 G. Surendran, L. Ramos, B. Pansu, E. Prouzet, P. Beaunier, F. Audonnet and H. Remita, *Chem. Mater.*, 2007, **19**, 5045–5048.
10 Y. Yamauchi, A. Sugiyama, R. Morimoto, A. Takai and K. Kuroda, *Angew. Chem. Int. Ed.*, 2008, **47**, 5371–5373.
11 D. Ruan, F. Gao and Z. Gu, *J. Electrochem. Soc.*, 2014, **161**, 666–671.
12 Y. Su, H. Liu, Z. Yan, M. Feng, J. Tang and H. Du, *Electrochim. Acta*, 2015, **164**, 182–186.
13 S. Garbarino, A. Ponrouch, S. Pronovost, J. Gaudet and D. Guay, *Electrochem. Commun.*, 2009, **11**, 1924–1927.
14 L. Liu, E. Pippel, R. Scholz and U. Gösele, *Nano Lett.*, 2009, 6876–6877.
15 Y. Sakamoto, A. Fukuoka, T. Higuchi, N. Shimomura, S. Inagaki and M. Ichikawa, *J. Phys. Chem. B*, 2004, **108**, 853–858.
16 A. Fukuoka and M. Ichikawa, *Top. Catal.*, 2006, **40**.
17 Y. Doi, A. Takai, Y. Sakamoto, O. Terasaki, Y. Yamauchi and K. Kuroda, *Chem. Commun.*, 2010, **46**, 6365–6367.
18 R. Ryoo, C. H. Ko, M. Kruk, V. Antochshuk and M. Jaroniec, *J. Phys. Chem. B*, 2000, **104**, 11465–11471.
19 C. H. Ko and R. Ryoo, *Chem. Commun.*, 1996, **1**, 2467–2468.
20 F. Kleitz, S. H. Choi and R. Ryoo, *Chem. Commun.*, 2003, 2136–2137.
21 H. J. Shin, R. Ryoo, Z. Liu and O. Terasaki, *J. Am. Chem. Soc.*, 2001, **123**, 1246–1247.
22 H. J. Shin, C. H. Ko and R. Ryoo, *J. Mater. Chem.*, 2001, **11**, 260–261.
23 Z. Liu, Y. Sakamoto, T. Ohsuna, K. Hiraga, O. Terasaki, C. H. Ko, H. J. Shin and R. Ryoo, *Angew. Chem. Int. Ed.*, 2000, **39**, 3107–3110.
24 A. Galarneau, H. Cambon, F. Di Renzo, R. Ryoo, M. Choi and F. Fajula, *New J. Chem.*, 2002, **27**, 73–79.
25 H. Wang, M. Imura, Y. Nemoto, S.-E. Park and Y. Yamauchi, *Chem. Asian J.*, 2012, **7**, 802–808.
26 H. Liu, D. Ma and X. Bao, *Dalton Trans.*, 2009, 1894–1896.
27 O. Terasaki, Z. Liu, T. Ohsuna, H. J. Shin and R. Ryoo, *Microsc. Microanal.*, 2002, **8**, 35–39.
28 H. Wang, H. Y. Jeong, I. Masataka, L. Wang, L. Radhakrishnan, N. Fujita, T. Castle, O. Terasaki and Y. Yamauchi, *J. Am. Chem. Soc.*, 2011, **133**, 14526–14529.
29 Y. Song, R. M. Garcia, R. M. Dorin, H. Wang, Y. Qiu, E. N. Coker, W. A. Steen, J. E. Miller and J. A. Shelnut, *Nano Lett.*, 2007, **7**, 3650–3655.
30 Y. Han, J. M. Kim and G. D. Stucky, *Chem. Mater.*, 2000, 2068–2069.
31 A. Fukuoka, T. Higuchi, T. Ohtake, T. Oshio, J. I. Kimura, Y. Sakamoto, N. Shimomura, S. Inagaki and M. Ichikawa, *Chem. Mater.*, 2006, **18**, 337–343.
32 B. C. Yang, H. Sheu and K. Chao, *Adv. Funct. Mater.*, 2002, **300**, 143–148.
33 X.-J. Guo, C.-M. Yang, P.-H. Liu, M.-H. Cheng and K.-J. Chao, *Cryst. Growth Des.*, 2005, **5**, 33–36.
34 C. Detavernier, J. Dendooven, S. Pulinthanathu Sree, K. F. Ludwig and J. A. Martens, *Chem. Soc. Rev.*, 2011, **40**, 5242–5253.
35 S. P. Sree, J. Dendooven, T. I. Koranyi, G. Vanbutsele, K. Houthoofd, D. Deduytsche, C. Detavernier and J. A. Martens, *Catal. Sci. Technol.*, 2011, 218–221.
36 S. P. Sree, J. Dendooven, J. Jammaer, K. Masschaele, D. Deduytsche, J. D. Haen, C. E. A. Kirschhock, J. A. Martens and C. Detavernier, *Chem. Mater.*, 2012, **24**, 2775–2780.
37 B. D. J. Comstock, S. T. Christensen, J. W. Elam, M. J. Pellin and M. C. Hersam, *Adv. Funct. Mater.*, 2010, **20**, 3099–3105.
38 J. Dendooven, R. K. Ramachandran, K. Devloo-Casier, G. Rampelberg, M. Filez, H. Poelman, G. B. Marin, E. Fonda and C. Detavernier, *J. Phys. Chem. C*, 2013, **117**, 20557–20561.
39 S. Deng, M. Kurttepeli, S. Deheryan, D. J. Cott, P. M. Vereecken, J. A. Martens, S. Bals, G. van Tendeloo and C. Detavernier, *Nanoscale*, 2014, **6**, 6939–6944.
40 H. Lee, S. H. Baeck, T. F. Jaramillo and S. F. Bent, *Nano Lett.*, 2013, **13**, 457–463.
41 A. Chen and P. Holt-hindle, *Chem. Rev.*, 2010, **110**, 3767–3804.
42 A. Fukuoka, N. Higashimoto, Y. Sakamoto, M. Sasaki, N. Sugimoto, S. Inagaki, Y. Fukushima and M. Ichikawa, *Catal. Today*, 2001, **66**, 23–31.
43 X. Zhang, W. Lu, J. Da, H. Wang, D. Zhao and P. a Webley, *Chem. Commun.*, 2009, 195–197.
44 N. K. Gopalan, S. Zhang, D. Du, P. Li and J. Ouyang, *ChemCatChem*, 2015, **7**, 422–426.
45 C. E. A. Kirschhock, S. P. B. Kremer, J. Vermant, G. Van Tendeloo, P. A. Jacobs and J. A. Martens, *Chem. Eur. J.*, 2005, **11**, 4306–4313.
46 J. A. Martens, J. W. Thybaut, J. F. . Denayer, S. P. Sree, A. Aerts, M. F. Reyniers, V. Van Speybroeck, M. Waroquier, A. Buekenhoudt, I. Vankelecom, W. Buijs, J. Persoons, G. V. Baron, S. Bals, G. Van Tendeloo, G. B. Marin, P. A. Jacobs and C. E. A. Kirschhock, *Catal. Today*, 2011, **168**, 17–27.
47 S. Bals, K. J. Batenburg, D. Liang, O. Lebedev, G. Van, A. Aerts, J. A. Martens and C. E. a Kirschhock, *J. Am. Chem. Soc*, 2009, **131**, 4769–4773.
48 W. Liu, E. Hu, H. Jiang, Y. Xiang, Z. Weng, M. Li, Q. Fan, X. Yu, E. I. Altman and H. Wang, *Nat. Commun.*, 2016, **7**, 10771.
49 A. Kiani and S. Hatami, *Int. J. Hydrogen Energy*, 2010, **35**, 5202–5209.
50 D. V. Esposito, S. T. Hunt, A. L. Stottlemyer, K. D. Dobson, B. E. McCandless, R. W. Birkmire and J. G. Chen, *Angew. Chem. Int. Ed.*, 2010, **49**, 9859–9862.
51 Y. Cao, Y. Yang, Y. Shan, C. Fu, N. Viet Long, Z. Huang, X. Guo and M. Nogami, *Nanoscale*, 2015, **7**, 19461–19467.
52 M. Carmo, D. L. Fritz, J. Mergel and D. Stolten, *Int. J. Hydrogen Energy*, 2013, **38**, 4901–4934.
53 M. T. M. Koper, *Nanoscale*, 2011, **3**, 2054–2073.
54 E. Skulason, V. Tripkovic, M. E. Bjorketun, S. Gudmundsdottir, G. Karlberg, J. Rossmeisl, T. Bligaard, H. Jonsson and J. K. Norskov, *J. Phys. Chem. C*, 2010, **114**, 18182–18197.
55 J. H. Barber and B. E. Conway, *J. Electroanal. Chem.*, 1999, **461**, 80–89.
56 N. M. Marković, B. N. Grgur and P. N. Ross, *J. Phys. Chem. B*, 1997, **101**, 5405–5413.
57 C. Burda, X. Chen and R. Narayanan, *Chem. Rev.*, 2005, **105**,

2–5.
58 B. E. Conway and B. V Tilak, *Electrochim. Acta*, 2002, **47**.
59 L. C. Gontard, R. E. Dunin-Borkowski and D. Ozkaya, *J. Microsc.*, 2008, **232**, 248–259.
60 S. E. F. Kleijn, S. C. S. Lai, M. T. M. Koper and P. R. Unwin, *Angew. Chem. Int. Ed.*, 2014, **53**, 3558–3586.
61 J. M. Petroski, Z. . l. Wang, T. . C. Green and M. A. El-Sayed, *J. Phys. Chem. B*, 1998, **102**, 3316–3320.
62 Y. Xia, Y. Xiong, B. Lim and S. E. Skrabalak, *Angew. Chem. Int. Ed.*, 2009, **48**, 60–103.
63 Y. T. Kim, K. Ohshima, K. Higashimine, T. Uruga, M. Takata, H. Suematsu and T. Mitani, *Angew. Chem. Int. Ed.*, 2006, **45**, 407–411.
64 N. Tian, Z.-Y. Zhou and S.-G. Sun, *J. Phys. Chem. C*, 2008, **112**, 19801–19817.
65 S. A. Desai, J. D. Rolston, L. Guo and S. M. Potter, *Front. Neuroeng.*, 2010, **3**, 1–5.
66 A. Norlin, J. Pan and C. Leygraf, *Biomol. Eng.*, 2002, **19**, 67–71.
67 W. Franks, I. Schenker, P. Schmutz and A. Hierlemann, *IEEE Trans. Biomed. Eng.*, 2005, **52**, 1295–1302.
68 S. F. Cogan, J. Ehrlich, T. D. Plante, A. Smirnov, D. B. Shire, M. Gingerich and J. F. Rizzo, in *Conf Proc IEEE Eng Med Biol Soc.*, 2004, vol. 6, pp. 4153–4156.
69 J. D. Weiland, D. J. Anderson and M. S. Humayun, *IEEE Trans. Biomed. Eng.*, 2002, **49**, 1574–1579.
70 E. W. Keefer, B. R. Botterman, M. I. Romero, A. F. Rossi and G. W. Gross, *Nat. Nanotechnol.*, 2008, **3**, 434–439.
71 K. A. Ludwig, J. D. Uram, J. Yang, D. C. Martin and D. R. Kipke, *J. Neural Eng.*, 2006, **3**, 59–70.
72 S. P. Sree, J. Dendooven, D. Smeets, D. Deduytsche, A. Aerts, K. Vanstreels, M. R. Baklanov, J. W. Seo, K. Temst, A. Vantomme, C. Detavernier and J. A. Martens, *J. Mater. Chem.*, 2011, **21**, 7692.

Table of contents entry

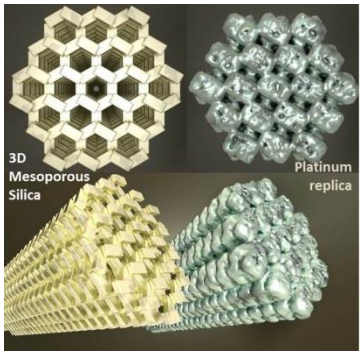

3D Porous Nanostructured Platinum Prepared via replicating the porosity of a 3D mesoporous silica material using Atomic Layer Deposition